Experimental Neurology 354 (2022) 114113

Contents lists available at ScienceDirect

Experimental Neurology

journal homepage: www.elsevier.com/locate/yexnr

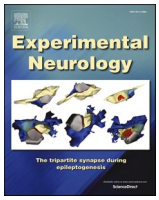

Research paper

Myelinated axons are the primary target of hemin-mediated oxidative damage in a model of the central nervous system

Karl Baldacchino [a], William J. Peveler [b], Leandro Lemgruber [c], Rebecca Sherrard Smith [a], Cornelia Scharler [d], Lorna Hayden [a], Lina Komarek [a], Susan L. Lindsay [a], Susan C. Barnett [a], Julia M. Edgar [a], Christopher Linington [a], Katja Thümmler [a,*]

[a] Institute of Infection, Immunity and Inflammation, University of Glasgow, G12 8TA Glasgow, United Kingdom
[b] WestCHEM, School of Chemistry, University of Glasgow, Joseph Black Building, G12 8QQ Glasgow, UK
[c] Glasgow Imaging Facility, Institute of Infection, Immunity and Inflammation, University of Glasgow, University Avenue, Glasgow G12 8QQ, UK
[d] Institute of Experimental and Clinical Cell Therapy, Paracelsus Medical University, Salzburg, Austria

ARTICLE INFO

Keywords:
Multiple sclerosis
Iron toxicity
Hemin
Protoporphyrin
Myelin
Axons

ABSTRACT

Iron released from oligodendrocytes during demyelination or derived from haemoglobin breakdown products is believed to amplify oxidative tissue injury in multiple sclerosis (MS). However, the pathophysiological significance of iron-containing haemoglobin breakdown products themselves is rarely considered in the context of MS and their cellular specificity and mode of action remain unclear. Using myelinating cell cultures, we now report the cytotoxic potential of hemin (ferriprotoporphyrin IX chloride), a major degradation product of haemoglobin, is 25-fold greater than equimolar concentrations of free iron in myelinating cultures; a model that reproduces the complex multicellular environment of the CNS. At low micro molar concentrations (3.3 - 10 μM) we observed hemin preferentially binds to myelin and axons to initiate a complex detrimental response that results in targeted demyelination and axonal loss but spares neuronal cell bodies, astrocytes and the majority of oligodendroglia. Demyelination and axonal loss in this context are executed by a combination of mechanisms that include iron-dependent peroxidation by reactive oxygen species (ROS) and ferroptosis. These effects are microglial-independent, do not require any initiating inflammatory insult and represent a direct effect that compromises the structural integrity of myelinated axons in the CNS. Our data identify hemin-mediated demyelination and axonal loss as a novel mechanism by which intracerebral degradation of haemoglobin may contribute to lesion development in MS.

1. Introduction

Multiple sclerosis (MS) is a chronic disease of the central nervous system (CNS) in which repeated episodes of inflammatory demyelination result in persistently demyelinated plaques of gliotic scar tissue associated with varying degrees of axonal injury and loss. This axonal pathology is generally considered a consequence of the local inflammatory response as this alone is sufficient to compromise the functional and structural integrity of affected axons. However, immunomodulatory treatments that suppress inflammatory activity in the CNS slow, but do not abolish accumulation of disability. This indicates inflammatory demyelination is not the sole driver of axonal pathology in MS and implies other mechanisms contribute to lesion development, but their identity and clinical relevance remain obscure.

Recent studies demonstrate oxidative stress and associated mitochondrial damage play important roles in driving axonal pathology in MS, and there is mounting circumstantial evidence that their effects are amplified by localised accumulation of iron in MS lesions (Filippi et al., 2019; Hametner et al., 2018; Hametner et al., 2013; Mahad et al., 2015; Stankiewicz et al., 2014). Following early reports of iron accumulating in MS brain tissue (Craelius et al., 1982; LeVine, 1997), alterations in the distribution of iron in and around MS lesions were confirmed by MRI, histopathology and synchrotron X-ray fluorescence imaging (Bagnato et al., 2011; Pitt et al., 2010; Popescu et al., 2017). Iron accumulates in the healthy brain during ageing (Hallgren and Sourander, 1958) and interestingly, those areas with the highest levels, such as thalamus, hypothalamus and basal ganglia, are preferentially affected by atrophy and neurodegeneration early in MS (Lansley et al., 2013). In addition,

* Corresponding author at: University of Glasgow, Institute of Infection, Immunity and Inflammation, 120 University Place, G12 8TA Glasgow, UK.
E-mail address: katja.thuemmler@glasgow.ac.uk (K. Thümmler).

https://doi.org/10.1016/j.expneurol.2022.114113
Received 5 January 2022; Received in revised form 29 April 2022; Accepted 8 May 2022
Available online 13 May 2022

accumulation of iron in basal ganglia correlates with disease progression and increased morphological damage in MS (Khalil et al., 2011).

Iron is essential for many basic biochemical processes necessary for brain development and function including cellular metabolism, mitochondrial function and oxygen transport, as well as neurotransmitter synthesis and myelination (Todorich et al., 2009). However, excess iron can compromise cellular function and survival due to its ability to promote the formation of reactive oxygen species (ROS) *via* the Fenton/Haber-Weiss reaction cycle. Neurons are thought to be particularly susceptible to oxidative damage due to their high levels of oxygen consumption and enrichment in polyunsaturated fatty acids (Núñez et al., 2012) (Gutteridge, 1992); a concept that extends to the myelin-axonal unit which is also metabolically highly active and enriched in long chain polyunsaturated membrane lipids. Indeed, accumulation of oxidised lipids correlates with iron loading in a subset of MS lesions supporting a causal association between iron availability and oxidative damage at these sites (Hametner et al., 2013). However, the origin of iron in MS lesions and how it contributes to lesion development remains unclear.

Most iron in the healthy brain is stored in oligodendrocytes and myelin (Connor and Menzies, 1995) and will be liberated during active demyelination (Hametner et al., 2013). This might locally overwhelm mechanisms responsible for maintaining iron homeostasis, raising the possibility free iron becomes available to mediate or amplify oxidative injury. However, iron can also accumulate in the CNS as a consequence of haemoglobin break-down following neuroinflammation-related vascular damage (Adams, 1988; Bagnato et al., 2011; Singh and Zamboni, 2009). The toxicity of haemoglobin and its break down products is well recognised in the context of intracerebral haemorrhage but its potential role in MS has attracted little attention. Nonetheless, not only are haemoglobin levels raised in patient CSF (Magliozzi et al., 2019) and serum (Lewin et al., 2016) but severity of disability correlates with the frequency of cerebral micro-bleeds (Zivadinov et al., 2016). These observations led us to speculate haemoglobin and its breakdown products, rather than iron *per se,* play the more important role in lesion development in some patients.

Hemin (ferriprotoporphyrin IX chloride) is an important haemoglobin break down product that is not only cytotoxic for isolated astrocytes (Dang et al., 2011a; Laird et al., 2008; Owen et al., 2016), neurons (Dang et al., 2011b; Zhou et al., 2017; Zille et al., 2017) and oligodendrocytes (Bamm et al., 2015), but also damages myelin lipids and proteins (MBP) (Bamm et al., 2017; Bamm et al., 2015) and induces a pro-inflammatory response in microglia/macrophages (Mehta et al., 2013; Sayeed et al., 2017). These effects contribute to tissue damage following haemorrhagic stroke, a situation in which haemoglobin breakdown may result in millimolar concentrations of hemin being reached in and around lesions (Robinson et al., 2009). However, hemin availability will be far lower in and around MS lesions and it is unclear if this will be sufficient to induce tissue damage in the complex, multicellular environment of the CNS. To address this, we investigated the effects of hemin in myelinating cultures derived from embryonic spinal cord, a model system that replicates the cellular complexity and many functional properties of the CNS *in vivo* (Bijland et al., 2019).

Low micromolar concentrations of hemin (3.3–10 μM) were found to preferentially associate with myelin and axons to initiate demyelination and axonal loss whilst sparing neuronal soma, astrocytes and a majority of oligodendrocytes. Crucially, we found hemin is significantly more toxic than free iron as 10 μM hemin induced extensive demyelination and axonal loss, whilst this concentration of $FeCl_3$ failed to induce any detrimental effect in this model system. We propose these effects are due to the hydrophobic nature of the porphyrin ring that allows hemin to interact with and/or intercalate into myelin and axons to initiate iron-dependent, ROS-mediated peroxidation of membrane lipids and proteins. This detrimental response occurs spontaneously in the absence of any inflammatory insult and is microglial-independent. Our data support a scenario in which hemin-dependent mechanisms are sufficient to initiate demyelination and axonal injury following micro haemorrhages in MS and other neurological diseases.

2. Material and methods

2.1. Myelinating cultures

To establish *in vitro* myelinating cultures, neurosphere-derived astrocytes were generated as described previously (Lindner et al., 2015). In brief, striata of post-natal day 1 *Sprague-Dawley* rats were dissociated and resuspended in 20 mL neurosphere media (DMEM/F12 containing 4.5 g/mL glucose, supplemented with 0.105% $NaHCO_3$, 2 mM glutamine, 1% penicillin/streptomycin, 5.0 mM HEPES, 0.0001% bovine serum albumin, 25 μg/mL human insulin, 100 μg/mL human apotransferrin, 60 μM putrescine, 20 nM progesterone, and 30 nM sodium selenite [all from Merck]) supplemented with 20 ng/mL mouse submaxillary gland epidermal growth factor (EGF, R&D Systems) in a 75 cm^3 tissue culture flask. After trituration into a single cell suspension, cells were plated on poly-L-lysine (13 μg/mL, Merck) coated 13 mm cover slips (VWR International) in low glucose DMEM supplemented with 10% foetal bovine serum and cultured until they formed a confluent monolayer. A single cell suspension of embryonic day 15.5 rat spinal cord cells (150,000 per cover slip) was then plated on the neurosphere-derived astrocyte monolayer in differentiation medium [DMEM (4.5 g/mL glucose), 10 ng/mL biotin, 0.5% N1 supplement, 50 nM hydrocortisone, and 0.1 μg/mL insulin (all from Merck)]. Twelve days later, insulin was omitted from the culture medium to promote myelination. Cultures were fed two to three times a week by replacing half the culture medium with fresh differentiation media and maintained at 37 °C/7% CO_2. Cultures were used once maximum myelination rates were established (day *in vitro* [DIV] 28), and prior to hemin/$FeCl_3$ treatment, apotransferin was withdrawn from cell cultures. Cultures were treated with the following components as detailed in the text: hemin, protoporphyrin IX, zinc (II) protoporphyrin IX (all Merck; dissolved as 1000× stock in dimethyl sulfoxide [DMSO]), or Iron (III) chloride (Merck, as 40× stock in 0.44 M L-ascorbic acid). DMSO or L-ascorbic acid were used as vehicle controls for porphyrins or iron (III) chloride respectively and did not have any detrimental effect on its own. For microglia depletion, cultures were treated from DIV18–28 with 1 μM PLX3397 (Selleckchem). To block specific pathways, cultures were treated at the same time as hemin with the following inhibitors: 250 μM deferoxamine mesylate (R&D Systems), 100 μM 4-Hydroxy-TEMPO (TEMPOL, Merck) as 100× stock in water and 2 μM ferrostatin-1 (Merck) as 1000× stock in DMSO.

To determine cytotoxicity induced by different compounds, cell culture supernatants were harvested at different time points (see figure legends) and lactate dehydrogenase (LDH) release was measured using the CytoTox 96® Non-Radioactive Cytotoxicity Assay (Promega) according to manufacturer's instructions.

2.2. Spinal cord explant cultures

Longitudinal *ex vivo* spinal cord slice cultures from one day old C57/B6 mice were prepared as previously described (Sekizar and Williams, 2019). In brief, after removing meninges the spinal cords were cut longitudinally at 300 μM thickness with a tissue chopper and transferred onto 0.4 μm millicell®-CM low height culture plate inserts with 1 mL slice culture media (40% minimal essential media, 40% horse serum, 25% Earl's balanced salt solution, 1% Pen/Strep, 1 x Glutamax and 2.6 mg/mL glucose) in the bottom of the well. Cultures were fed every two days by replacing all the culture medium and maintained at 37 °C/7% CO_2. After 14 days, cultures were treated with 10 μM hemin or vehicle control for 24 h. Thereafter slices were washed twice with PBS, fixed with 4% paraformaldehyde for 1 h at room temperature and permeabilized with 100% ethanol for 20 min at −20 °C. Primary antibodies (SMI-31 [1:1000, mouse IgG1, Biolegend], AA3 [1:100, PLP/DM20

specific, rat IgG] and GFAP [1:500, rabbit IgG, Merck]) were incubated for 48 h at 4 °C in blocking buffer (1 mM HEPES, 2% heat inactivated horse serum, 10% heat inactivated goat serum, 1% bovine serum albumin and 0.25% TritonX in HBSS), followed by washing three times with 0.05% TritonX/PBS and incubation with species/isotype specific secondary antibodies (1:400) for 3 h at room temperature. For every biological replicate, 20 random images per spinal cord slice of two slices per condition were taken for quantitative analysis at 63× magnification using a Zeiss LSM 880 confocal microscope. Myelin ensheathment (PLP), axonal density (SMI31) and pixel intensities for GFAP were automatically quantified using CellProfiler cell image analysis software with in-house developed pipelines: (https://github.com/muecs/cp/blob/v1.3/slice_cultures.cpproj). For the quantification of myelination rates, pipelines only quantify PLP positive myelin sheaths whilst round myelin positive structures (such as myelinating cells or myelin debris) are automatically filtered out based on their shape. For representative images z-stacks were obtained (maximum intensity projection).

2.3. Immunocytochemistry

After treatment with hemin/$FeCl_3$, myelinating cultures were fixed in 4% paraformaldehyde (PFA) for 15 min at room temperature, permeabilised with 0.5% Triton-X/PBS for 15 min and blocked for at least 30 min in PBS/10% Horse serum/1% bovine serum albumin, followed by primary antibody incubation for 45 min (see list below) and by incubation with isotype/species specific secondary antibodies (15 min in the dark). Then cover slips were washed (PBS followed by distilled water) and mounted with Mowiol 4–88 (33% *w/v* Mowiol® 4–88, 13.2% w/v glycerol [both Merck], 0.05% *v*/v DAPI [Invitrogen] in 0.13 M Tris pH 8.5 [Calbiochem]). For surface staining (Hemin and O4 antibody), live cells were first incubated with primary antibody (30 min, 4 °C) and afterwards fixed with 4% PFA.

Primary antibodies were used as following: SMI-31 (1:1000, mouse IgG1, Biolegend), Z2 (1:500, MOG-specific, mouse IgG2a, (Piddlesden et al., 1993)), MBP (1:400, rat IgG, Biorad), β tubulin III (1:200, mouse IgG2a, Merck), NeuN (1:400, Millipore), Nestin (1:200, mouse IgG1 Millipore), 4-Hydroxynonenal (1:200, mouse IgG1, ThermoFisher), GFAP (1:500, rabbit IgG, Merck), O4 (1:500, mouse IgM, R&D Systems), Olig2 (1:200, mouse IgG2a, Millipore), Iba1 (1:500, Wako), Hemin (1:10, mouse IgM, absolute antibody), AA3 (1:200, PLP/DM20 specific, rat IgG, (Yamada et al., 1999)). Species and isotype specific secondary antibodies labelled with Alexa Fluor 488, Alexa Fluor 568 or Alexa Fluor 647 (Invitrogen) were used at 1:400. For every biological replicate, 10 random images per coverslip of three coverslips per condition were taken for quantitative analysis at 10× magnification (neurite density and myelination) or 20× magnification (cell counts) using an Olympus BX51 fluorescent microscope with a Retiga R6 and Ocular software (QImaging) or using the Zeiss Axio Imager 2 and Zen blue software. Representative confocal images were obtained at 40× magnification (LD C-Apochromat 40×/1.1 W Zeiss objective) using a Zeiss LSM 880 confocal microscope (2% laser light; z-stack of 10 slices with 1 μm each) and Zen Black software. Myelination (MOG) was analysed from 10× images with Fiji adopted from https://github.com/BarnettLab/MyelinJ (Whitehead et al., 2019). Myelination (MBP), NeuN counts and pixel intensities for GFAP, nestin and 4-HNE were automatically quantified using CellProfiler cell image analysis software (Carpenter et al., 2006). The pipelines used here were developed in-house and are available at https://github.com/muecs/cp/tree/v1.3. Olig2, PLP and Iba1 cell counts were manually quantified in a blinded fashion.

2.4. Fluorescence spectroscopy and direct visualization of hemin via fluorescence microscopy

Hemin (chloroprotoporphyrin IX iron(III), Merck) was dissolved at 60 nM in DMSO and fluorescence spectra with variable excitation wavelength were recorded on a Horiba Duetta Bio spectrometer with 3 nm bandpass filter on excitation and emission, a 0.5 nm resolution for emission (on CCD) and 2 nm step for excitation respectively; integration time per excitation wavelength was 2 s. Data is represented as 2D map of emission wavelength (x) *vs* excitation wavelength (y) *vs* emission intensity (z).

For direct visualization of hemin, cultures were treated with 10 μM hemin for 3, 12 or 24 h and then stained for SMI31, MOG, MBP, O4 and Iba-1 as described above, but not incubated with DAPI. Secondary antibodies for these markers were a combination of species/isotype specific Alexa Fluor 488, Alexa Fluor 568 or Alexa Fluor 647 (Invitrogen). The direct detection of hemin binding in cell culture, was implemented according to the obtained fluorescence spectra by measuring emission between 420 and 450 nm at an excitation of 385–405 nm. Images were obtained at 20× (UPlanFL 20×/0.5 Olympus objective) on a widefield DeltaVision Core microscope (AppliedPrecision) with SoftWorx software. Slices of 0.2 μm were acquired, to a total of 2 μm in thickness. The out-of-focus light was removed through deconvolution, using the default set-up in the same software.

2.5. Scanning electron microscopy

To visualize myelinated axons by scanning EM, hemin-treated or control cultures were live stained for the myelin marker MOG (1:80) for 30 min at 4 °C and afterwards fixed with 4% PFA. After washing and blocking for at least 30 min with PBS/10% Horse serum/1% bovine serum albumin, cells were incubated with gold-labelled mouse secondary antibody (1:10, from Aurion, Netherlands), washed, dehydrated in ascending series of ethanol, and critical point dried (Tousimis, USA). The dried samples were coated with gold/palladium (10 nm thick layer) and imaged in a JEOL IT-100 scanning electron microscope (Jeol, Japan). Gold labeling was observed using the backscattered detector.

2.6. Transcriptional data

RNA was extracted from DIV28 myelinating control cultures or cells treated with 3 or 10 μM hemin for 24 h using the Qiagen RNeasy Micro kit according to manufacturer's instructions. RNA yields and quality were determined by nanodrop. For transcriptional screening, 1 μg RNA per condition was transcribed using the RT^2 First Strand Kit (Qiagen) followed by the RT^2 Profiler PCR Array "Rat Cytokines & Chemokines" (Qiagen) according to the manufacturer's instructions.

To validate changes in selected candidates from PCR Array screening, quantitative real-time PCR was performed on cultures treated as mentioned above. After RNA extraction, cDNA was synthesized with the QuantiTect® Reverse Transcription Kit (Qiagen) following the manufacturer's instructions using a Biometra T3 Thermocycler (Thermofisher) with the following parameters: first cycle at 42 °C for 2 min; after adding reverse transcriptase, primer mix and reaction buffer second, cycle at 42 °C for 20 min, then 3 min for 95 °C. Primers for real-time PCR were designed with Primer 3 software (http://biotools.umassmed.edu/bioapps/primer3_www.cgi) (Rozen and Skaletsky, 2000) and specificity checked with BLAST (http://blast.ncbi.nlm.nih.gov/Blast.cgi). Real-time PCR was performed in triplicates for each sample using 10 ng cDNA template, 1× SYBR Green master mix (Applied Biosystems), and 50 pmol/μL of each primer (purchased from IDT, sequences shown in Supplementary Table 1) in an Applied Biosystems Fast Real-Time PCR System (ABI 7500) using the following settings: 50 °C for 5 min, 95 °C for 10 min, followed by 40 cycles at 95 °C for 15 s, 60 °C for 1 min, and the final dissociation step at 95 °C for 15 s. The $2^{-\Delta CT}$ method (Schmittgen and Livak, 2008) was used to determine differences in gene expression (*gapdh* as housekeeping gene). One-way ANOVA was performed on ΔCT values for each experimental repeat to test for significant changes of 3.3 μM hemin or 10 μM hemin treated cultures compared to untreated cultures.

2.7. Protein quantification

Myelinating cultures (DIV28) were treated with different concentrations of hemin and after 24 h supernatants were harvested. Protein concentrations of CXCL1 and CCL2 in the cell culture supernatants were measured using CXCL1/KC or CCL2/JE/MCP-1 Quantikine ELISA kits (both R&D Systems) according to the manufacturer's instructions.

For quantification of 4-HNE/ western blotting, cell lysates were prepared in RIPA lysis buffer with protease inhibitors (cOmplete Protease Inhibitor Cocktail, Roche) and protein concentration was quantified with BCA Protein AssaySystem (Pierce). The cytoplasmic fraction of cell lysates was then used to quantify 4-HNE levels by ELISA using the Lipid Peroxidation (4-HNE) Assay Kit (abcam) according to manufacturer's instructions. 4-HNE levels were then normalized to total protein amount for each sample. For western blotting, protein samples were denatured with NuPAGE LDS sample buffer/sample reducing agent (Invitrogen) at 70 °C for ten minutes. 10 μg of protein were run on 4–12% gradient NuPAGE bis-tris acrylamide gels (Invitrogen) at 200 V for 45–60 min and transferred using iBlot (Invitrogen) to a PVDF membrane. Membranes were blocked in 5% skimmed milk in Tris-buffered saline/0.01% tween (TBS/T; pH 7.4) for 1 h and incubated overnight with the following primary antibodies at 4 °C: SMI31 (1:10,000; ms IgG1, Biolegend), neurofilament light (1:1000; rabbit IgG; Merck), GFAP (1:10,000; rabbit IgG; Dako) and β actin as loading control (1:1000; msIgG1; Merck). After thorough washing, membranes were incubated with horseradish peroxidase (HRP) conjugated goat anti-mouse or goat anti-rabbit secondary antibodies (1:10,000; CellSignaling) for 1 h, and after washing developed using the WesternBright ECL system (Advansta). Bands were visualized using the C-DiGit Blot Scanner (Li-COR) and intensities were quantified using ImageJ software.

2.8. Statistical analysis

Statistical analysis was performed with GraphPad Prism 7 (GraphPad Software Inc) using paired *t*-tests or one-way ANOVA with post-hoc tests as specified in the text. For each experiment, the number of n values is specified in the according figure legend and each n value represents a single independent cell culture, comprising multiple coverslips (technical repeats). A p-value <0.05 was considered statistically significant, with $p < 0.001$ ***; $p < 0.01$ **; $p < 0.05$ *; n.s. = not significant.

2.9. Data availability

The Fiji plugin for myelin quantification can be found at https://github.com/BarnettLab/MyelinJ and CellProfiler pipelines can be found at https://github.com/muecs/cp/tree/v1.2. All other data supporting the findings of this study are available in the article and the supplementary information files, or from the corresponding author upon reasonable request.

3. Results

3.1. Hemin preferentially targets the myelin-axon unit

To explore the pathogenic potential of hemin in the CNS, we utilized myelinating cultures derived from embryonic rat spinal cord that replicate the cellular complexity of the CNS *in vivo*. Using lactate dehydrogenase (LDH) release as a global measure of cytotoxicity we found treating myelinated cultures (DIV 28) for 24 h with hemin (≥3.3 μM) resulted in significant cytotoxicity (24 h: 3.3 μM, 22.9% ± 4.5%; 10 μM, 36.8% ± 5.3%; 30 μM, 64.9% ± 4.7%; vehicle control, 5.1% ± 0.7%) (Fig. 1A) and an increase in pyknotic nuclei at higher hemin concentrations (Supplemental Fig. 1A). Treating cultures for 48 h (Supplemental Fig. 1B) led to further increases in LDH release at 3.3 μM and 10 μM hemin, whereas 0.33 μM hemin had no significant cytotoxic effect even if treatment was prolonged for up to 6 days (Fig. 1A & Supplemental Fig. 1C).

To determine if hemin preferentially targeted any specific cell type, its effects were investigated by immunofluorescence microscopy and western blotting using a variety of cell-specific markers. We observed myelin sheaths were extremely sensitive to damage by hemin (Fig. 1B, C). Immunofluorescence microscopy revealed demyelination was dose-dependent; 3.3 μM and 10 μM hemin mediating 50% and 75% demyelination (loss of MOG^+ immunoreactivity) after 24 h, respectively (Fig. 1C). Moreover, residual regions of MOG^+ ensheathment were highly fragmented and exhibited extensive blebs and swellings (Fig. 1B & Supplemental Fig. 1D). This pathology was accompanied by extensive axonal loss as demonstrated by immunofluorescence microscopy for phosphorylated neurofilament heavy chain (NF-H; SMI31) (Fig. 1B) and western blotting of NF-H, NF-M and NF-L (Fig. 1D & Supplemental Fig. 1E). The latter demonstrating all three neurofilament chains were reduced by >50% in cultures treated with 3.3 μM hemin for 24 h when compared to untreated cultures. These effects were confirmed by immunofluorescence microscopy for MBP and β-tubulin III, as myelin and neurite specific markers, respectively (Fig. 1E). Loss of MBP immune reactivity was extensive and was associated with extensive fragmentation of myelin sheaths and swellings similar to that observed- using MOG as a myelin marker, whilst the linear staining pattern characteristic of β-tubulin III^+ neurites was lost completely (Fig. 1E & Supplemental Fig. 1D/F).

To visualize this pathology directly, we utilized scanning electron microscopy of myelinating cultures in which the outermost surface of myelin sheaths was labelled using a MOG-specific primary antibody in combination with a gold-labelled isotype/species-specific secondary antibody (Fig. 1F). In untreated cultures myelinated axons appeared as smooth tubular structures expressing MOG on their surface, but following treatment with 10 μM hemin for 24 h this architecture was largely disrupted (Fig. 1F). Loss of myelin and neurites was even more pronounced in cultures treated with 30 μM hemin in which cellular damage/loss was so extensive, virtually no neurites were detectable by scanning electron microscopy (Supplemental Fig. 1G).

3.2. Neurons and astrocytes are resistant to damage by low hemin concentrations

Hemin-induced demyelination was accompanied by loss of both $Olig2^+$ glia, as well as more mature PLP^+ oligodendrocytes which decreased by 44% and 21%, respectively (Fig. 2A; $Olig2^+$ cells: 10 μM, 56.3 ± 5.5; vehicle control, 100.9 ± 8.8 for; PLP^+ cells: 10 μM, 25.5 ± 1.4; vehicle control, 32.4 ± 0.8 cells per field of view). In striking contrast, although 3.3 μM or 10 μM hemin induced extensive axonal loss after 24 h, this was not accompanied by any significant reduction in the number of $NeuN^+$ neurons in this time frame (Fig. 2B) or over a prolonged time of up to 5 days of hemin treatment (Supplemental Fig. 2A). Similarly, astrocytes also appear largely spared after 24 h as demonstrated by immunofluorescence (Fig. 2C) and western blotting for GFAP (Supplemental Fig. 2B), although a slight increase in nestin immune reactivity suggests on going astrocyte activation (Clarke et al., 1994) (Sahin Kaya et al., 1999); Supplemental Fig. 2C. A similarly targeted effect of hemin was also observed in *ex vivo* spinal cord slice cultures. Of interest, 10 μM hemin treatment for 24 h already resulted in significant loss of axons and myelin sheaths (48% and 50% respectively), while astrocytes are not affected by hemin treatment (Supplemental Fig. 2D/E).

3.3. Hemin-cytotoxicity is microglial independent

In view of the important role played by microglia in many neurodegenerative diseases e. g. in the clearance of myelin debris after injury (Neumann et al., 2008), we next asked if hemin cytotoxicity was microglia-dependent in this model system. Treatment with 10 μM hemin resulted in a significant decrease in $Iba1^+$ microglia (Fig. 2D, 10 μM,

43.2 ± 5.3; vehicle control, 64.5 ± 5.8 cells per field of view), but the majority of Iba1$^+$ cells survived to adopt a rounded, amoeboid morphology indicative of microglial activation (Fig. 2D). To determine if this microglial response was itself cytotoxic, we investigated the effect of microglial depletion on hemin-induced LDH release. Pre-treating myelinated cultures with PLX3397, a potent colony-stimulating factor 1 receptor (CSF1R) inhibitor, completely eliminated Iba1$^+$ microglia (Hayden et al., 2020) (Supplemental Fig. 3), but had no effect on hemin-mediated LDH release (Fig. 2E). This indicates hemin-mediated cytotoxicity is *per se* microglial independent. Nonetheless, screening cytokine and chemokine expression revealed hemin induced increased expression of multiple pro-inflammatory factors including C-X-C Motif Chemokine Ligand 1 (*CXCL1*), C-C Motif Chemokine Ligand 2 (*CCL2*), C-C Motif Chemokine Ligand 7 (*CCL7*), Leukemia inhibitory factor (*LIF*) and Interleukin 6 (*IL6*) as well as Growth Differentiation Factor 15 (*GDF15*) involved in the stress response to cellular injury (Fig. 3A; Supplemental Table 1 & Supplementary data set 1). These transcriptional data were validated for CCL2 (Fig. 3B) and CXCL1 (Fig. 3C) *via* ELISA, confirming hemin stimulated secretion of both chemokines. Moreover, analyses of supernatants harvested from PLX3397 pre-treated cultures revealed microglia were the main source of these chemokines (Fig. 3B & C). Hemin-mediated cytotoxicity is, therefore, microglial-independent *in vitro*, but we anticipate the accompanying "pro-inflammatory" microglial response will exacerbate neuroinflammation *in vivo*.

3.4. Hemin preferentially interacts with myelin and neurites

Having demonstrated hemin cytotoxicity is microglial-independent we speculated its selectivity for myelin, neurites, oligodendrocytes and microglia is a direct consequence of hemin binding to these targets. This was initially investigated using a hemin-specific antibody, but its sensitivity proved limited as we were only able to identify occasional hemin$^+$/Olig2$^+$ cells in cultures treated with the highest concentration of hemin (30 μM) (Fig. 4A & Supplemental Fig. 4A). To improve sensitivity, we turned to the intrinsic fluorescence properties of hemin that exhibits maximum absorption between 300 and 450 nm and a strong emission peak between 420 and 480 nm (Fig. 4B & Supplemental Fig. 4B). This enabled us to directly visualize bound hemin using an excitation wavelength of 385–405 nm and measure emission between 420 and 450 nm ("Hemin channel" - white, Fig. 4C & D) using a conventional fluorescent microscope. To our knowledge, this is the first report of direct hemin detection by fluorescent microscopy in cell culture, a strategy that proved more sensitive than classical immunofluorescence microscopy. Analysis of cultures treated with 10 μM hemin for 12 h, not only identified hemin co-localizing in oligodendrocytes (O4$^+$ cells; purple), but also with myelin sheaths (MOG; green) and axons (SMI31; red) (Fig. 4C). Hemin binding colocalizing with myelin sheaths (MBP, green) could already be observed after 3 h treatment with hemin and before any damage to myelin or axons was apparent (Supplemental Fig. 4C). After 24 h the hemin signal redistributed to co-localize mainly with residual fragmented myelin and Iba1$^+$ microglia, a distribution reflecting the extent of neurite loss and demyelination at this time point (Fig. 4D).

3.5. Mechanistic basis of hemin cytotoxicity

As an initial step towards determining how hemin damages myelin and neurites, we aimed to establish if free iron was similarly efficient at mediating demyelination and axonal loss. This was not the case. Whilst 10 μM hemin was highly toxic, equimolar concentrations of $FeCl_3$ failed to induce either demyelination or axonal loss (Fig. 5A). This is in contrast to a far higher concentration of $FeCl_3$ (250 μM) that can induce extensive demyelination and neurite loss in this culture model. This led us to speculate that the hydrophobic porphyrin ring of hemin may plays a critical role in mediating hemin cytotoxicity due to its ability to intercalate into lipid membranes (Man et al., 2011), an effect predicted to target hemin to sites sensitive to oxidative damage. To test this, we compared the cytotoxic potential of hemin to that of protoporphyrin IX ("hemin without iron") and Zn^{2+} protoporphyrin IX. Neither protoporphyrin IX nor Zn^{2+} protoporphyrin IX were cytotoxic (Fig. 5B), demonstrating iron is in fact required to mediate the cytotoxic effect of hemin in these cultures.

We then investigated the role of ferroptosis as a mechanism contributing to hemin cytotoxicity. However, inhibiting this pathway with the ferrostatin-1 (Dixon et al., 2012) only partially reduced hemin induced cytotoxicity in cultures treated with 3.3 μM hemin but had no significant effect in cultures treated with higher concentrations (Fig. 5C), an observation demonstrating ferroptosis is not a major factor contributing to hemin cytotoxicity in this model system. This is in line with observations that iron chelation (250 μM deferoxamine mesylate) had some effect on hemin induced cytotoxicity/demyelination only at the lower hemin concentration of 3.3 μM (Supplemental Fig. 4D/E). As hemin is predicted to preferentially oxidise membrane lipids containing long polyunsaturated fatty acid chains, we then investigated whether cellular damage was associated with enhanced lipid peroxidation. We observed an increase in the peroxidation product, 4-Hydroxynonenal (4-HNE) immune reactivity in cultures treated with 10 μM hemin for 24 h (Fig. 5D), an observation confirmed by ELISA for cytoplasmic 4-HNE (Fig. 5E). To conclusively establish a role for ROS in hemin cytotoxicity, we compared LDH release after hemin treatment in the absence or presence of TEMPOL, a free radical scavenger with antioxidant properties. TEMPOL reduced cytotoxicity by approximately 40% in cultures treated with 3.3 μM ($p < 0.05$) and 10 μM ($p < 0.01$) hemin (Fig. 5F, 3.3 μM: 16.5% ± 2.5% with TEMPOL *vs* 28.8% ± 3.5% without TEMPOL and 10 μM: 21.8% ± 4.4% with TEMPOL *vs* 35.5% ± 4.4% without TEMPOL), demonstrating that the detrimental effects of hemin in myelinating cultures are not only porphyrin- and iron-dependent but involve a significant contribution from ROS-dependent mechanisms.

4. Discussion

Understanding the mechanistic basis underlying demyelination and axonal loss in MS is essential if we are to generate fully effective treatments for this devastating disease. In response to speculation whether haemoglobin and/or its break down products exacerbate tissue damage (Bamm et al., 2017) (Lewin et al., 2016), we compared the cytotoxic potential of iron and hemin in an *in vitro* model of the CNS. We found micromolar concentrations of hemin (3.3–10 μM) selectively mediated demyelination and axonal loss in this model system, but spared neuronal cell bodies, astrocytes as well as the majority of PLP$^+$ oligodendrocytes and microglia. This degree of selectivity was unexpected as previous studies using monocultures of CNS cells demonstrate hemin is not only cytotoxic for oligodendrocytes, but also isolated astrocytes (Owen et al., 2016) and neurons (Goldstein et al., 2003).

We attribute this target specificity to a combination of effects. First, immune and direct fluorescent microscopy demonstrated hemin binds preferentially to myelin, axons, a population of oligodendrocytes, and, only at later time points, also co-localised with microglia. We suggest binding to myelin and other membranes is facilitated by the hydrophobic nature of the porphyrin ring that enables hemin to intercalate into and/or bind to membrane surfaces (Giri et al., 2018) (Schmitt et al., 1993). Once intercalated into a membrane bilayer hemin is not only protected from degradation by heme-oxygenases and sequestration by hemin-binding proteins such as hemopexin, but is also ideally located to initiate peroxidation of membrane proteins and long chain polyunsaturated lipids (Schmitt et al., 1993) (Bamm et al., 2017). Immune fluorescence and ELISA for 4-HNE confirmed hemin-induced peroxidation, an effect predicted to result in destabilisation and destruction of affected structures, in this case the myelin sheath and axon. Susceptibility of oligodendrocytes, myelin and axons will be further amplified by factors such as high levels of intracellular iron (Reinert et al., 2019) and polyunsaturated fatty acids (DeVries et al., 1981), as well as intrinsically

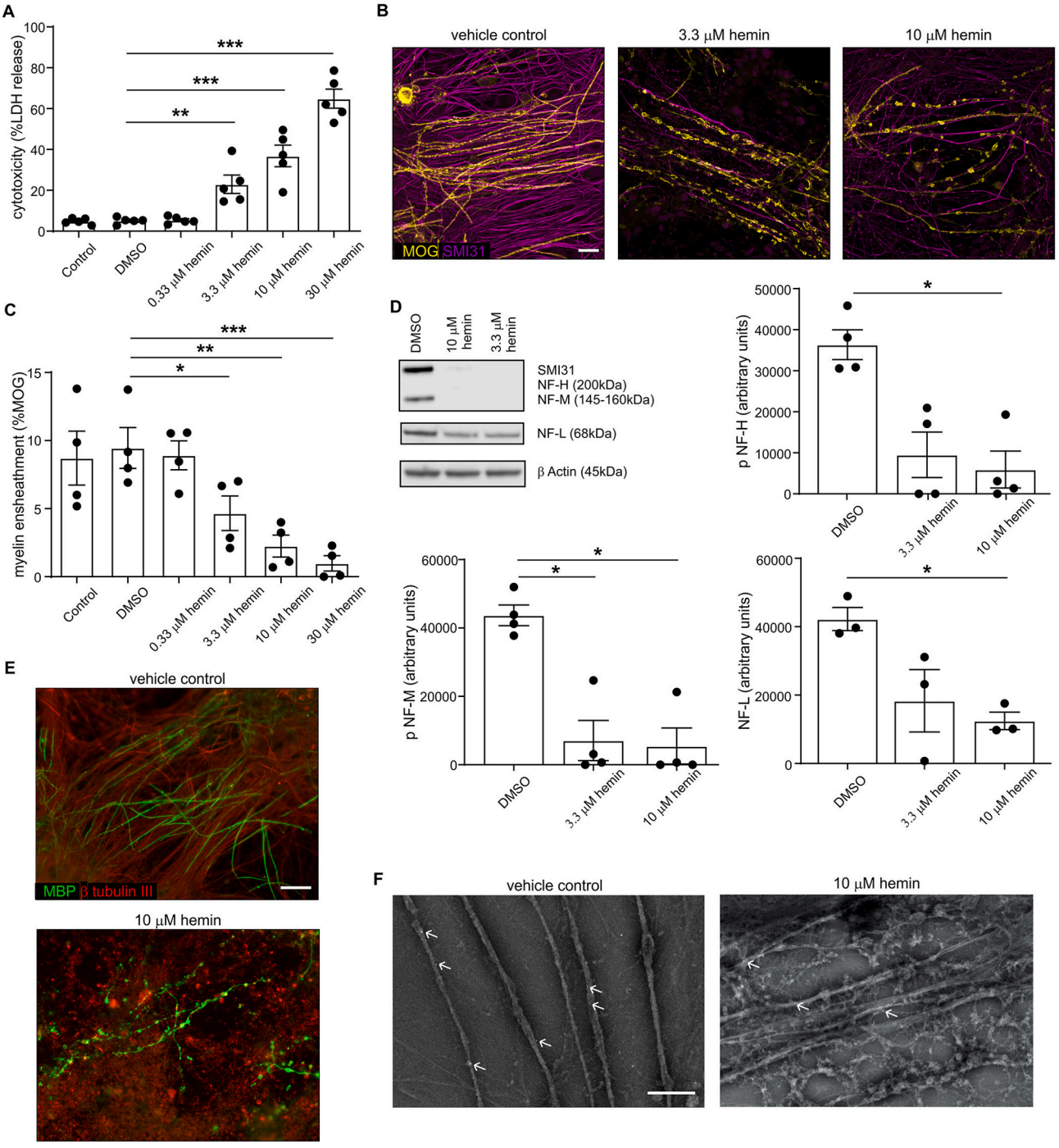

Fig. 1. Hemin preferentially targets the myelin/axon unit. Rat myelinating spinal cord cultures were treated with different concentrations of hemin (0.3–30 μM) or DMSO (vehicle control) at DIV28 for 24 h, (A) treatment with 3.3–30 μM hemin significantly increased cytotoxicity (LDH release in cell culture supernatants). Shown are mean ± SEM of five independent experiments; one-way ANOVA with Tukey's post-test; $^{**}p < 0.01$, $^{***}p < 0.001$. Fully myelinated cell cultures with a well-established network of axons (DIV28) were treated with different concentrations of hemin for 24 h: (B, C) immunofluorescence staining for myelin sheaths (MOG, yellow) and axons (SMI31, magenta) reveals a detrimental effect of 3.3–30 μM hemin on the integrity of both the myelin sheath and axons, (B) shown are representative confocal images (maximum intensity projection, scale bar: 20 μm). (C) The amount of intact myelin sheaths is significantly reduced in cultures treated with 3.3–30 μM hemin; mean ± SEM of four independent experiments; one-way ANOVA with Tukey's post-test; $^{*}p < 0.05$, $^{**}p < 0.01$, $^{***}p < 0.001$. (D) Treatment with hemin results in a marked reduction of neurofilament levels as assessed by western blot. Shown are representative blots for untreated and hemin treated cultures; cell lysates (cytoplasmic fraction) were probed for phosphorylated neurofilament heavy and medium chain (SMI31, double band on top blot) and neurofilament light chain (NF-L antibody, middle plot) in comparison to β actin loading control (bottom blot). Hemin treatment results in a significant reduction in the amount of neurofilament heavy, medium and light chain protein; mean ± SEM of at least three independent experiments, one-way ANOVA with Tukey's post-test, $^{*}p < 0.05$. (E) Probing for another marker of mature myelin (MBP, green) and axons (β tubulin III, red) reveals a similar detrimental effect on the myelin/axon unit; representative images, scale bar: 50 μm. (F) Scanning electron microscopy of DIV 28 myelinating cultures treated with 10 μM hemin for 24 h and labelled for myelin surface expression with MOG antibody and gold-conjugated species/isotype specific secondary antibody shows disintegration of axons (long tubular structures with smooth surface in the untreated cultures); MOG expression as visualized by gold labelling is indicated by white arrows and is localised on the axon surface; scale bar: 5 μm. (For interpretation of the references to colour in this figure legend, the reader is referred to the web version of this article.)

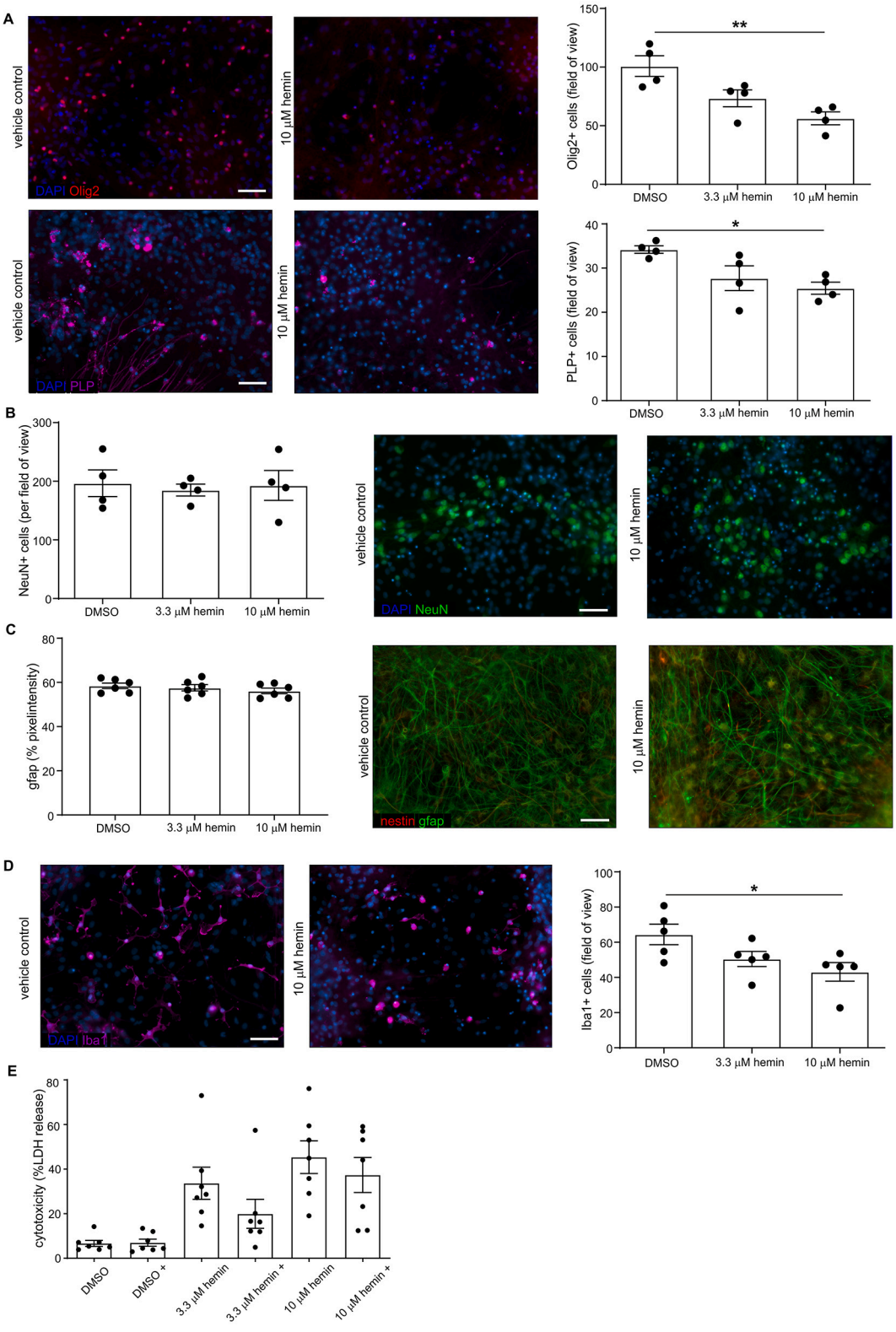

(caption on next page)

Fig. 2. Neurons and astrocytes are resistant to damage by low hemin concentrations. (A) 10 μM hemin significantly reduces the number of oligodendrocytes (Olig2$^+$, PLP$^+$) after 24 h in myelinating cell culture (DIV28); left panel shows representative images of Olig2$^+$ (top, red) and PLP$^+$ oligodendrocytes (bottom, magenta), scale bar: 50 μm. Quantification of oligodendrocyte (Olig2$^+$ or PLP$^+$ cells) numbers show a significant reduction after treatment with 10 μM hemin; mean ± SEM of four independent experiments, one-way ANOVA with Tukey's post-test, *$p < 0.05$, **$p < 0.01$. (B, C) 24-h treatment of myelinating cultures with 3.3 and 10 μM hemin has no effect on neuronal soma (B, NeuN, green) or astrocyte densities (C, GFAP, green). Left panels show mean ± SEM of at least four independent experiments, one-way ANOVA with Tukey's post-test. Right panels: representative images for neuronal soma (B: NeuN, green) and astrocytes (C: GFAP, green); scale bar: 50 μm. (D) DIV28 myelinated cultures treated with 10 μM hemin show a significant reduction in microglia numbers (Iba1$^+$) after 24 h of treatment; representative images of Iba1$^+$ microglia (magenta), scale bar: 50 μm. Quantification of microglia (Iba1$^+$ cell) numbers show a significant reduction after hemin treatment; mean ± SEM of five independent experiments, one-way ANOVA with Tukey's post-test, *$p < 0.05$. (E) Myelinating cultures were treated with hemin or vehicle control in the absence or presence of a colony-stimulating factor 1 receptor (CSF-1R) inhibitor PLX3397 (1 μM from DIV18–28; designated as "+"), which almost completely depletes microglia in these cultures. After 24 h of hemin treatment, supernatants were harvested and analysed for LDH release. As shown previously, 3.3 and 10 μM hemin treatment resulted in an increased LDH release. This hemin-induced cytotoxicity was, however, not significantly reduced in microglia depleted cultures (designated as "+"); shown are mean ± SEM of seven independent experiments. (For interpretation of the references to colour in this figure legend, the reader is referred to the web version of this article.)

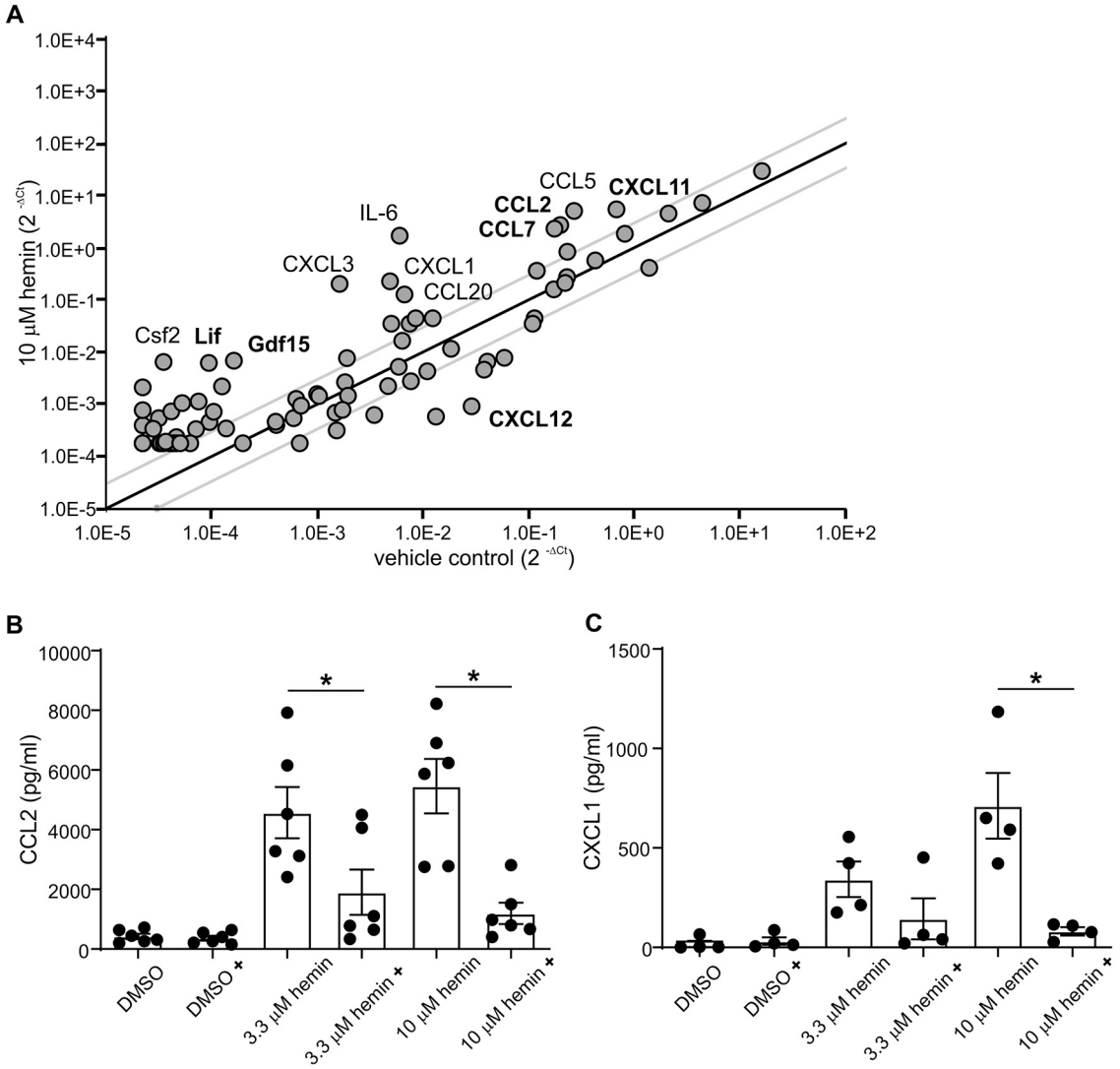

Fig. 3. Hemin treatment induces a pro-inflammatory phenotype in microglia. (A) DIV28 myelinating cultures (3 independent biological repeats per treatment group) were treated with 10 μM hemin for 24 h and transcript levels of 84 rat cytokines/chemokines were determined by RT^2 Profiler PCR Arrays "Rat Cytokines & Chemokines". This reveals an up-regulation of a variety of pro-inflammatory cytokines and chemokines after hemin treatment; shown is the $2^{-\Delta Ct}$ scatter plot of treatment (10 μM Hemin, y-axis) *vs* control (x-axis) group, black line indicates fold change of 1 and grey lines a fold change of +/− 3; bold: genes validated by qPCR. (B, C) Myelinating cultures were treated with hemin or vehicle control in the absence or presence of the potent microglia inhibitor Pexidartinib (PLX3397, 1 μM from DIV18–28; designated as "+"), which leads to almost complete depletion of microglia in these cultures. After 24 h of hemin treatment, supernatant was harvested and CCL2 (B) and CXCL1 (C) levels determined by ELISA. Both treatment with 3.3 or 10 μM hemin significantly increase CCL2 and CXCL1 secretion and this is dependent on the presence of microglia in the myelinating cultures; shown are mean ± SEM of at least four independent experiments, one-way ANOVA with Tukey's post-test,* $p < 0.05$.

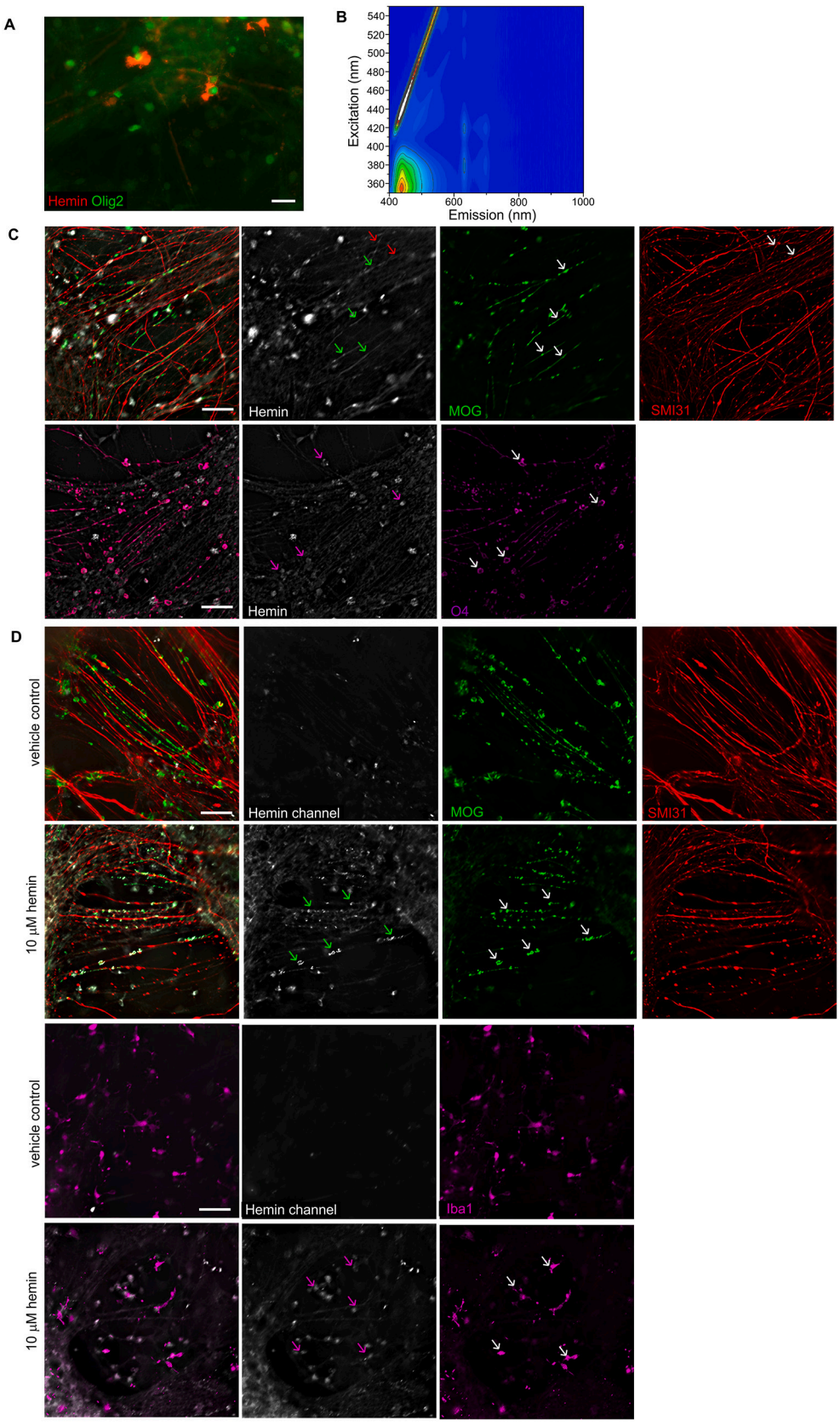

Fig. 4. Hemin preferentially interacts with myelin and neurites. Rat myelinating spinal cord cultures were treated with different concentrations of hemin (0.3–30 μM) or DMSO (vehicle control) at DIV28. (A) Hemin antibody binding (red) to cell surface co-localizes with Olig2 expression (green) after 30 min treatment of myelinating cultures with 30 μM hemin; scale bar: 20 μm. (B) Excitation/Emission map of hemin luminescence, from a 60 nM hemin solution in DMSO. A clear emission peak is observed at 420–480 nm, excited maximally at 350–390 nm. The diagonal line seen in the upper left quadrant results from Rayleigh scattering of the excitation light, and porphyrin emission is weakly observed at 630 and 700 nm. (C, D) Fluorescent properties of hemin were utilized for direct detection of hemin binding in cell culture, by imaging emission between 420 and 450 nm at an excitation of 385–405 nm ("Hemin channel, white") in combination with conventional fluorescent signal for myelin sheets (MOG, green), axons (SMI31, red), oligodendrocyte lineage cells (O4, magenta) or microglia (Iba1, magenta). (C) Confocal images (maximum intensity projection) of DIV28 myelinating cultures treated with 10 μM hemin for 12 h show hemin preferentially binds to myelin sheets (green arrows), oligodendrocytes (magenta arrows) and, to some extent, to axons (red arrows); scale bar: 50 μm. (D) After treatment with 10 μM hemin for 24 h hemin binds to myelin fragments (green arrows) and, to some extent, to microglia (magenta arrows); note: untreated cultures show only a very weak background signal in the "Hemin channel" compared to hemin treated cultures due to some auto fluorescence of cells; scale bar: 50 μm. (For interpretation of the references to colour in this figure legend, the reader is referred to the web version of this article.)

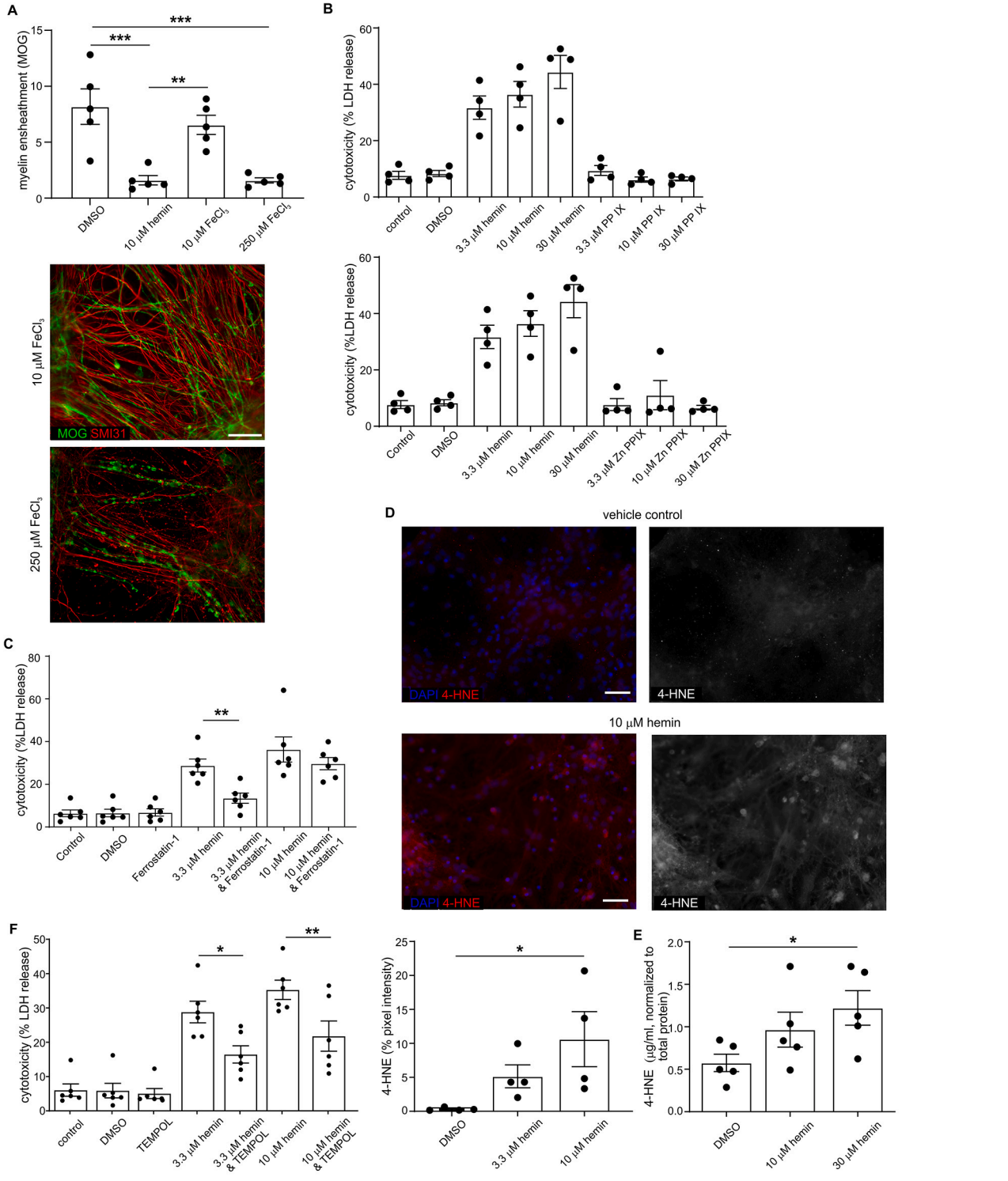

(caption on next page)

Fig. 5. Mechanistic basis of hemin cytotoxicity. (A) In myelinating cultures, 24-h treatment with 10 μM hemin results in a significant reduction of intact myelin sheaths, whereas equimolar concentrations of $FeCl_3$ has no detrimental effect on the myelin/axon unit. It requires much higher concentrations of $FeCl_3$ (250 μM) to induce damage similar to that seen after treatment with 10 μM hemin. Top panel: mean ± SEM for quantification of myelin ensheathment of five independent experiments; one-way ANOVA with Tukey's post-test; $^{**}p < 0.01$, $^{***}p < 0.001$; bottom panel: representative immune-fluorescence images for myelin (MOG, green) and axons (SMI31, red) after treatment with different concentrations of $FeCl_3$, scale bar: 20 μm. (B) 3.3–30 μM hemin treatment induces increased LDH release, whereas equimolar concentrations of protoporphyrin IX (PPIX, "Hemin without iron"; top panel) or Zn^{2+} protoporphyrin IX (Zn PPIX; bottom panel) do not result in an increased cytotoxicity; LDH release shown as mean ± SEM of four independent experiments. (C) Myelinating cultures were treated with 3.3 or 10 μM hemin or vehicle control in the absence or presence of a ferroptosis inhibitor (2 μM ferrostatin-1) and after 24 h of treatment, LDH release was assessed. The ferroptosis inhibitor could partly inhibit the cytotoxic effect of 3.3 μM hemin, but had only a minor effect in the 10 μM hemin treatment group. Shown are mean ± SEM of six independent experiments, one-way ANOVA with Tukey's post-test, $^{**}p < 0.01$. (D, E) Hemin exposure increases lipid peroxidation as assessed by increase in the lipid peroxidation product 4-Hydroxynonenal (4-HNE). Treatment with 10 μM hemin for 24 h significantly increases 4-HNE expression; (D) representative immunofluorescence staining for 4-HNE (red on left; white on right), scale bar: 50 μm; (D, bottom left): quantification of 4-HNE expression by immunofluorescence, mean ± SEM of four independent experiments, one-way ANOVA with Tukey's post-test,* $p < 0.05$. (E) quantification of cytoplasmic 4-HNE *via* ELISA, mean ± SEM of five independent experiments, one-way ANOVA with Tukey's post-test,* $p < 0.05$. (F) The presence of 100 μM TEMPOL, a membrane-permeable free radical scavenger with antioxidant properties, significantly reduces cytotoxicity induced by 3.3 or 10 μM hemin (24 h treatment of DIV28 myelinating cultures); mean ± SEM of six independent experiments, one-way ANOVA with Tukey's post-test,* $p < 0.05$, $^{**}p < 0.01$. (For interpretation of the references to colour in this figure legend, the reader is referred to the web version of this article.)

low levels of glutathione and other antioxidant defence mechanisms (Thorburne and Juurlink, 1996) (Juurlink et al., 1998) (French et al., 2009) and high metabolic rate/oxygen consumption. This may explain why myelin, oligodendrocytes and axons are the compartments most susceptible to oxidative damage after partial transection of the optic nerve (Giacci and Fitzgerald, 2018), as well as in active MS lesions (Haider et al., 2011). However, why myelin and axonal loss are not accompanied by a corresponding loss of neurons in our *in vitro* model remains unclear. Mechanistically this may be related to Wallerian degeneration in which activation of sterile alpha and TIR motif-containing protein 1 (SARM1) promotes axonal degeneration whilst it is attenuated by nicotinamide mononucleotide adenylyltransferase (NMNAT) (Conforti et al., 2014) (Coleman and Höke, 2020) (Figley et al., 2021). However, it should be noted that acute axonal injury is not necessarily associated with Wallerian degeneration in MS or its animal model, experimental autoimmune encephalitis (EAE) (Singh et al., 2017). Furthermore, acute axonal damage in EAE is mediated by reactive oxygen and nitrogen species (Sorbara et al., 2014) and when disease is induced in mice carrying the Wallerian degeneration slow (*Wld* ^{S}) mutation this pathology is largely unaffected (Singh et al., 2017).

In addition to passive uptake, hemin is also actively imported into cells *via* heme transporters, such as heme carrier protein 1 (HCP-1), heme responsive gene-1 (HRG-1) and divalent metal transporter 1 (DMT-1) (Rajagopal et al., 2008; Yanatori et al., 2010), and by endocytosis of hemin scavengers, such as haptoglobin or hemopexin (Donegan et al., 2019) (Ascenzi et al., 2005). All these heme transporters are transcriptionally expressed in the CNS, albeit at different levels in neurons, oligodendroglia, astrocytes and microglia (Zhang et al., 2014). Functionally, HCP-1 contributes to hemin uptake by astrocytes and neurons (Dang et al., 2010) (Dang et al., 2011b) whilst HRG-1 is highly expressed in myelinating oligodendrocytes (Zhang et al., 2014) where it might function as an endosomal heme transporter (O'Callaghan et al., 2010) (Yanatori et al., 2010). It is tempting to speculate HRG-1 expression contributes to the susceptibility of oligodendrocytes and myelin to hemin-mediated injury. However, we suggest when present at low levels, cellular import of hemin is more likely to result in detoxification through intracellular degradation and subsequent recycling/sequestration of its degradation products; a mechanism that may contribute to the inability of low concentrations of hemin to kill neurons and astrocytes in this study. Furthermore, others demonstrated astrocytes are consistently more resistant to the detrimental effects of iron and hemin than oligodendrocytes or neurons *in vitro* (Regan and Panter, 1993; Zhang et al., 2005) (Chen-Roetling and Regan, 2006) (Kress et al., 2002) (Oshiro et al., 2008). This may be due to robust astrocytic expression of several iron efflux proteins which limit their ability to accumulate iron (Zarruk et al., 2015), as well as high levels of antioxidative mediators such as heme oxygenase-1 and peroxisome proliferator-activated receptor gamma coactivator 1 (Chen-Roetling et al., 2005; Nijland et al., 2014) (Xu et al., 2016; Yu et al., 2016). In the case of microglial uptake of hemin, this may be *via* the heme transporters HCP-1 and DMT-1 or alternatively, due to phagocytosis of hemin-containing myelin debris. We currently favour the latter as significant numbers of $hemin^{+}$ microglia were only detected once cultures were actively demyelinating.

On a mechanistic level, we demonstrated hemin-induced cytotoxicity is iron-dependent, as neither PPIX nor zinc-substituted PPIX induced significant LDH release in myelinated cultures. However, complexing Fe^{3+} within the protoporphyrin ring clearly amplifies its cytotoxic potential, as much higher concentrations of $FeCl_3$ were required to initiate a similar degree of demyelination and axonal loss. Similar findings were reported using astrocyte cultures, in which hemin or lipophilic iron compounds were also significantly more toxic than free iron (Owen et al., 2016) (Robb and Connor, 1998). In this context, hemin's protoporphyrin ring not only allows it to intercalate into membrane bilayers, but also appears to stabilize soluble Fe^{2+} whereas treatment with non-hemin iron results in accumulation of insoluble Fe^{3+} within cells (Owen et al., 2016). Lipid peroxidation products, as assessed by monitoring 4-HNE, can be then explained by Fe^{2+} mediated formation of ROS and autocatalytic oxidation of membrane lipids (Ayala et al., 2014). To confirm ROS production plays a significant role in hemin-induced cytotoxicity, we investigated the effects of TEMPOL, an antioxidant and free radical scavenger, on hemin-induced cytotoxicity. TEMPOL inhibited hemin-induced LDH release by 40%, an effect similar to that reported for astrocytes (Laird et al., 2008). This confirms ROS play a central role in hemin-induced cytotoxicity, but we wish to stress this represented only one facet of a multifactorial process that involve contributions from other mechanisms including ferroptosis.

Depleting cultures of microglia prior to hemin treatment demonstrated its cytotoxicity in this *in vitro* model is microglial-independent. Nonetheless, hemin does activate microglia as demonstrated by their adopting an amoeboid morphology and expression of pro-inflammatory mediators in this and other studies (Zhang et al., 2006) (Sayeed et al., 2017) (Lin et al., 2012). Our data indicate that whilst this response is not cytotoxic *per se*, the associated induction of pro-inflammatory chemokines will promote immune cell recruitment and lesion development *in vivo*. This raises questions as to the functional significance of iron-laden microglia observed at the rim of active MS lesions which has led to speculation they contribute to lesion development (Dal-Bianco et al., 2017) (Zrzavy et al., 2017) (Mehta et al., 2013). Is this actually true, or is this increase in microglial iron an epiphenomenon reflecting sequestration and detoxification of iron derived from haemoglobin and/or oligodendrocytes?

In summary, we demonstrate hemin, a major haemoglobin breakdown product, mediates demyelination and axonal loss in an *in vitro* model of the CNS. This detrimental effect is highly selective, involves iron-dependent stimulation of ROS production and lipid peroxidation

and occurs at concentrations at which free iron has no cytotoxic effect. These findings lend further support to the hypothesis haemoglobin break down products contribute to lesion development in MS and other neurological diseases.

Author contributions

K. T., C. S., S. C. B, J. M. E., and C. L. conceived and designed research; K. B., C. S., R. S. S., W. J. P., L. K., L. L., L. H., S. L. L. and K. T. performed research; K. B., W. J. P., R. S. S., L. L. and K. T. collected and analysed data; K.T, and S. L. L. visualization; K. B., C. L., J. M. E. and K. T. wrote the paper; C. L. and K. T. secured funding.

Declaration of Competing Interest

The authors declare no competing interests.

Acknowledgments

This work was supported by funding from the United Kingdom Multiple Sclerosis Society (K. T., grant 58, C. L., J. M. E.); University of Glasgow LKAS Fellowship (W. J. P.); EPSRC ECR Capital Award EP/S017984/1 (PL instrumentation); Gemeinnützige Hertie Stiftung (C. L.); and TENOVUS (S20-06; K. T.). The authors gratefully acknowledge the Glasgow Imaging Facility for their support & assistance in this work; Dr. Hua Wang for his insightful comments on the manuscript; Dr. Michael Whitehead for providing the Fiji App to analyse myelination rates and Steve Muecklisch for developing CellProfiler pipelines for automatic image quantification.

Appendix A. Supplementary data

Supplementary data to this article can be found online at https://doi.org/10.1016/j.expneurol.2022.114113.

References

Adams, C.W., 1988. Perivascular iron deposition and other vascular damage in multiple sclerosis. J. Neurol. Neurosurg. Psychiatry 51, 260–265.
Ascenzi, P., Bocedi, A., Visca, P., Altruda, F., Tolosano, E., Beringhelli, T., Fasano, M., 2005. Hemoglobin and heme scavenging. IUBMB Life 57, 749–759.
Ayala, A., Muñoz, M.F., Argüelles, S., 2014. Lipid peroxidation: production, metabolism, and signaling mechanisms of malondialdehyde and 4-hydroxy-2-nonenal. Oxidative Med. Cell. Longev. 2014, 360438.
Bagnato, F., Hametner, S., Yao, B., van Gelderen, P., Merkle, H., Cantor, F.K., Lassmann, H., Duyn, J.H., 2011. Tracking iron in multiple sclerosis: a combined imaging and histopathological study at 7 tesla. Brain 134, 3602–3615.
Bamm, V.V., Lanthier, D.K., Stephenson, E.L., Smith, G.S., Harauz, G., 2015. In vitro study of the direct effect of extracellular hemoglobin on myelin components. Biochim. Biophys. Acta 1852, 92–103.
Bamm, V.V., Henein, M.E.L., Sproul, S.L.J., Lanthier, D.K., Harauz, G., 2017. Potential role of ferric hemoglobin in MS pathogenesis: effects of oxidative stress and extracellular methemoglobin or its degradation products on myelin components. Free Radic. Biol. Med. 112, 494–503.
Bijland, S., Thomson, G., Euston, M., Michail, K., Thümmler, K., Mücklisch, S., Crawford, C.L., Barnett, S.C., McLaughlin, M., Anderson, T.J., Linington, C., Brown, E.R., Kalkman, E.R., Edgar, J.M., 2019. An in vitro model for studying CNS white matter: functional properties and experimental approaches. F1000Res 8, 117.
Carpenter, A.E., Jones, T.R., Lamprecht, M.R., Clarke, C., Kang, I.H., Friman, O., Guertin, D.A., Chang, J.H., Lindquist, R.A., Moffat, J., Golland, P., Sabatini, D.M., 2006. CellProfiler: image analysis software for identifying and quantifying cell phenotypes. Genome Biol. 7, R100.
Chen-Roetling, J., Regan, R.F., 2006. Effect of heme oxygenase-1 on the vulnerability of astrocytes and neurons to hemoglobin. Biochem. Biophys. Res. Commun. 350, 233–237.
Chen-Roetling, J., Benvenisti-Zarom, L., Regan, R.F., 2005. Cultured astrocytes from heme oxygenase-1 knockout mice are more vulnerable to heme-mediated oxidative injury. J. Neurosci. Res. 82, 802–810.
Clarke, S.R., Shetty, A.K., Bradley, J.L., Turner, D.A., 1994. Reactive astrocytes express the embryonic intermediate neurofilament nestin. Neuroreport 5, 1885–1888.
Coleman, M.P., Höke, A., 2020. Programmed axon degeneration: from mouse to mechanism to medicine. Nat. Rev. Neurosci. 21, 183–196.
Conforti, L., Gilley, J., Coleman, M.P., 2014. Wallerian degeneration: an emerging axon death pathway linking injury and disease. Nat. Rev. Neurosci. 15, 394–409.
Connor, J.R., Menzies, S.L., 1995. Cellular management of iron in the brain. J. Neurol. Sci. 134 (Suppl), 33–44.
Craelius, W., Migdal, M.W., Luessenhop, C.P., Sugar, A., Mihalakis, I., 1982. Iron deposits surrounding multiple sclerosis plaques. Arch. Pathol. Lab. Med. 106, 397–399.
Dal-Bianco, A., Grabner, G., Kronnerwetter, C., Weber, M., Höftberger, R., Berger, T., Auff, E., Leutmezer, F., Trattnig, S., Lassmann, H., Bagnato, F., Hametner, S., 2017. Slow expansion of multiple sclerosis iron rim lesions: pathology and 7 T magnetic resonance imaging. Acta Neuropathol. 133, 25–42.
Dang, T.N., Bishop, G.M., Dringen, R., Robinson, S.R., 2010. The putative heme transporter HCP1 is expressed in cultured astrocytes and contributes to the uptake of hemin. Glia 58, 55–65.
Dang, T.N., Bishop, G.M., Dringen, R., Robinson, S.R., 2011a. The metabolism and toxicity of hemin in astrocytes. Glia 59, 1540–1550.
Dang, T.N., Robinson, S.R., Dringen, R., Bishop, G.M., 2011b. Uptake, metabolism and toxicity of hemin in cultured neurons. Neurochem. Int. 58, 804–811.
DeVries, G.H., Zetusky, W.J., Zmachinski, C., Calabrese, V.P., 1981. Lipid composition of axolemma-enriched fractions from human brains. J. Lipid Res. 22, 208–216.
Dixon, S.J., Lemberg, K.M., Lamprecht, M.R., Skouta, R., Zaitsev, E.M., Gleason, C.E., Patel, D.N., Bauer, A.J., Cantley, A.M., Yang, W.S., Morrison 3rd, B., Stockwell, B.R., 2012. Ferroptosis: an iron-dependent form of nonapoptotic cell death. Cell 149, 1060–1072.
Donegan, R.K., Moore, C.M., Hanna, D.A., Reddi, A.R., 2019. Handling heme: the mechanisms underlying the movement of heme within and between cells. Free Radic. Biol. Med. 133, 88–100.
Figley, M.D., Gu, W., Nanson, J.D., Shi, Y., Sasaki, Y., Cunnea, K., Malde, A.K., Jia, X., Luo, Z., Saikot, F.K., Mosaiab, T., Masic, V., Holt, S., Hartley-Tassell, L., McGuinness, H.Y., Manik, M.K., Bosanac, T., Landsberg, M.J., Kerry, P.S., Mobli, M., Hughes, R.O., Milbrandt, J., Kobe, B., DiAntonio, A., Ve, T., 2021. SARM1 is a metabolic sensor activated by an increased NMN/NAD(+) ratio to trigger axon degeneration. Neuron 109, 1118–1136.e1111.
Filippi, M., Brück, W., Chard, D., Fazekas, F., Geurts, J.J.G., Enzinger, C., Hametner, S., Kuhlmann, T., Preziosa, P., Rovira, À., Schmierer, K., Stadelmann, C., Rocca, M.A., 2019. Association between pathological and MRI findings in multiple sclerosis. Lancet Neurol. 18, 198–210.
French, H.M., Reid, M., Mamontov, P., Simmons, R.A., Grinspan, J.B., 2009. Oxidative stress disrupts oligodendrocyte maturation. J. Neurosci. Res. 87, 3076–3087.
Giacci, M., Fitzgerald, M., 2018. Oligodendroglia are particularly vulnerable to oxidative damage after neurotrauma in vivo. J. Exp. Neurosci. 12 (1179069518810004).
Giri, R.P., Mukhopadhyay, M.K., Basak, U.K., Chakrabarti, A., Sanyal, M.K., Runge, B., Murphy, B.M., 2018. Continuous uptake or saturation-investigation of concentration and surface-packing-specific hemin interaction with lipid membranes. J. Phys. Chem. B 122, 7547–7554.
Goldstein, L., Teng, Z.P., Zeserson, E., Patel, M., Regan, R.F., 2003. Hemin induces an iron-dependent, oxidative injury to human neuron-like cells. J. Neurosci. Res. 73, 113–121.
Gutteridge, J.M., 1992. Iron and oxygen radicals in brain. Ann. Neurol. 32 (Suppl), S16–S21.
Haider, L., Fischer, M.T., Frischer, J.M., Bauer, J., Höftberger, R., Botond, G., Esterbauer, H., Binder, C.J., Witztum, J.L., Lassmann, H., 2011. Oxidative damage in multiple sclerosis lesions. Brain 134, 1914–1924.
Hallgren, B., Sourander, P., 1958. The effect of age on the non-haemin iron in the human brain. J. Neurochem. 3, 41–51.
Hametner, S., Wimmer, I., Haider, L., Pfeifenbring, S., Brück, W., Lassmann, H., 2013. Iron and neurodegeneration in the multiple sclerosis brain. Ann. Neurol. 74, 848–861.
Hametner, S., Dal Bianco, A., Trattnig, S., Lassmann, H., 2018. Iron related changes in MS lesions and their validity to characterize MS lesion types and dynamics with ultra-high field magnetic resonance imaging. Brain Pathol. 28, 743–749.
Hayden, L., Semenoff, T., Schultz, V., Merz, S.F., Chapple, K.J., Rodriguez, M., Warrington, A.E., Shi, X., McKimmie, C.S., Edgar, J.M., Thümmler, K., Linington, C., Pingen, M., 2020. Lipid-specific IgMs induce antiviral responses in the CNS: implications for progressive multifocal leukoencephalopathy in multiple sclerosis. Acta Neuropathol. Commun. 8, 135.
Juurlink, B.H., Thorburne, S.K., Hertz, L., 1998. Peroxide-scavenging deficit underlies oligodendrocyte susceptibility to oxidative stress. Glia 22, 371–378.
Khalil, M., Langkammer, C., Ropele, S., Petrovic, K., Wallner-Blazek, M., Loitfelder, M., Jehna, M., Bachmaier, G., Schmidt, R., Enzinger, C., Fuchs, S., Fazekas, F., 2011. Determinants of brain iron in multiple sclerosis: a quantitative 3T MRI study. Neurology 77, 1691–1697.
Kress, G.J., Dineley, K.E., Reynolds, I.J., 2002. The relationship between intracellular free iron and cell injury in cultured neurons, astrocytes, and oligodendrocytes. J. Neurosci. 22, 5848–5855.
Laird, M.D., Wakade, C., Alleyne Jr., C.H., Dhandapani, K.M., 2008. Hemin-induced necroptosis involves glutathione depletion in mouse astrocytes. Free Radic. Biol. Med. 45, 1103–1114.
Lansley, J., Mataix-Cols, D., Grau, M., Radua, J., Sastre-Garriga, J., 2013. Localized grey matter atrophy in multiple sclerosis: a meta-analysis of voxel-based morphometry studies and associations with functional disability. Neurosci. Biobehav. Rev. 37, 819–830.
LeVine, S.M., 1997. Iron deposits in multiple sclerosis and Alzheimer's disease brains. Brain Res. 760, 298–303.
Lewin, A., Hamilton, S., Witkover, A., Langford, P., Nicholas, R., Chataway, J., Bangham, C.R.M., 2016. Free serum haemoglobin is associated with brain atrophy in secondary progressive multiple sclerosis. Wellcome Open Res 1, 10.

Lin, S., Yin, Q., Zhong, Q., Lv, F.L., Zhou, Y., Li, J.Q., Wang, J.Z., Su, B.Y., Yang, Q.W., 2012. Heme activates TLR4-mediated inflammatory injury via MyD88/TRIF signaling pathway in intracerebral hemorrhage. J. Neuroinflammation 9, 46.
Lindner, M., Thümmler, K., Arthur, A., Brunner, S., Elliott, C., McElroy, D., Mohan, H., Williams, A., Edgar, J.M., Schuh, C., Stadelmann, C., Barnett, S.C., Lassmann, H., Mücklisch, S., Mudaliar, M., Schaeren-Wiemers, N., Meinl, E., Linington, C., 2015. Fibroblast growth factor signalling in multiple sclerosis: inhibition of myelination and induction of pro-inflammatory environment by FGF9. Brain 138, 1875–1893.
Magliozzi, R., Hametner, S., Facchiano, F., Marastoni, D., Rossi, S., Castellaro, M., Poli, A., Lattanzi, F., Visconti, A., Nicholas, R., Reynolds, R., Monaco, S., Lassmann, H., Calabrese, M., 2019. Iron homeostasis, complement, and coagulation cascade as CSF signature of cortical lesions in early multiple sclerosis. Ann. Clin. Transl. Neurol. 6, 2150–2163.
Mahad, D.H., Trapp, B.D., Lassmann, H., 2015. Pathological mechanisms in progressive multiple sclerosis. Lancet Neurol. 14, 183–193.
Man, D., Słota, R., Broda, M.A., Mele, G., Li, J., 2011. Metalloporphyrin intercalation in liposome membranes: ESR study. J. Biol. Inorg. Chem. 16, 173–181.
Mehta, V., Pei, W., Yang, G., Li, S., Swamy, E., Boster, A., Schmalbrock, P., Pitt, D., 2013. Iron is a sensitive biomarker for inflammation in multiple sclerosis lesions. PLoS One 8, e57573.
Neumann, H., Kotter, M.R., Franklin, R.J.M., 2008. Debris clearance by microglia: an essential link between degeneration and regeneration. Brain 132, 288–295.
Nijland, P.G., Witte, M.E., van het Hof, B., van der Pol, S., Bauer, J., Lassmann, H., van der Valk, P., de Vries, H.E., van Horssen, J., 2014. Astroglial PGC-1alpha increases mitochondrial antioxidant capacity and suppresses inflammation: implications for multiple sclerosis. Acta Neuropathol. Commun. 2, 170.
Núñez, M.T., Urrutia, P., Mena, N., Aguirre, P., Tapia, V., Salazar, J., 2012. Iron toxicity in neurodegeneration. Biometals 25, 761–776.
O'Callaghan, K.M., Ayllon, V., O'Keeffe, J., Wang, Y., Cox, O.T., Loughran, G., Forgac, M., O'Connor, R., 2010. Heme-binding protein HRG-1 is induced by insulin-like growth factor I and associates with the vacuolar H+-ATPase to control endosomal pH and receptor trafficking. J. Biol. Chem. 285, 381–391.
Oshiro, S., Kawamura, K., Zhang, C., Sone, T., Morioka, M.S., Kobayashi, S., Nakajima, K., 2008. Microglia and astroglia prevent oxidative stress-induced neuronal cell death: implications for aceruloplasminemia. Biochim. Biophys. Acta 1782, 109–117.
Owen, J.E., Bishop, G.M., Robinson, S.R., 2016. Uptake and toxicity of hemin and Iron in cultured mouse astrocytes. Neurochem. Res. 41, 298–306.
Piddlesden, S.J., Lassmann, H., Zimprich, F., Morgan, B.P., Linington, C., 1993. The demyelinating potential of antibodies to myelin oligodendrocyte glycoprotein is related to their ability to fix complement. Am. J. Pathol. 143, 555–564.
Pitt, D., Boster, A., Pei, W., Wohleb, E., Jasne, A., Zachariah, C.R., Rammohan, K., Knopp, M.V., Schmalbrock, P., 2010. Imaging cortical lesions in multiple sclerosis with ultra-high-field magnetic resonance imaging. Arch. Neurol. 67, 812–818.
Popescu, B.F., Frischer, J.M., Webb, S.M., Tham, M., Adiele, R.C., Robinson, C.A., Fitz-Gibbon, P.D., Weigand, S.D., Metz, I., Nehzati, S., George, G.N., Pickering, I.J., Brück, W., Hametner, S., Lassmann, H., Parisi, J.E., Yong, G., Lucchinetti, C.F., 2017. Pathogenic implications of distinct patterns of iron and zinc in chronic MS lesions. Acta Neuropathol. 134, 45–64.
Rajagopal, A., Rao, A.U., Amigo, J., Tian, M., Upadhyay, S.K., Hall, C., Uhm, S., Mathew, M.K., Fleming, M.D., Paw, B.H., Krause, M., Hamza, I., 2008. Haem homeostasis is regulated by the conserved and concerted functions of HRG-1 proteins. Nature 453, 1127–1131.
Regan, R.F., Panter, S.S., 1993. Neurotoxicity of hemoglobin in cortical cell culture. Neurosci. Lett. 153, 219–222.
Reinert, A., Morawski, M., Seeger, J., Arendt, T., Reinert, T., 2019. Iron concentrations in neurons and glial cells with estimates on ferritin concentrations. BMC Neurosci. 20, 25.
Robb, S.J., Connor, J.R., 1998. An in vitro model for analysis of oxidative death in primary mouse astrocytes. Brain Res. 788, 125–132.
Robinson, S.R., Dang, T.N., Dringen, R., Bishop, G.M., 2009. Hemin toxicity: a preventable source of brain damage following hemorrhagic stroke. Redox Rep. 14, 228–235.
Rozen, S., Skaletsky, H., 2000. Primer3 on the WWW for general users and for biologist programmers. Methods Mol. Biol. 132, 365–386.
Sahin Kaya, S., Mahmood, A., Li, Y., Yavuz, E., Chopp, M., 1999. Expression of nestin after traumatic brain injury in rat brain. Brain Res. 840, 153–157.
Sayeed, M.S.B., Alhadidi, Q., Shah, Z.A., 2017. Cofilin signaling in hemin-induced microglial activation and inflammation. J. Neuroimmunol. 313, 46–55.
Schmitt, T.H., Frezzatti Jr., W.A., Schreier, S., 1993. Hemin-induced lipid membrane disorder and increased permeability: a molecular model for the mechanism of cell lysis. Arch. Biochem. Biophys. 307, 96–103.
Schmittgen, T.D., Livak, K.J., 2008. Analyzing real-time PCR data by the comparative C (T) method. Nat. Protoc. 3, 1101–1108.
Sekizar, S., Williams, A., 2019. Ex vivo slice cultures to study myelination, demyelination, and remyelination in mouse brain and spinal cord. Methods Mol. Biol. 1936, 169–183.
Singh, A.V., Zamboni, P., 2009. Anomalous venous blood flow and iron deposition in multiple sclerosis. J. Cereb. Blood Flow Metab. 29, 1867–1878.
Singh, S., Dallenga, T., Winkler, A., Roemer, S., Maruschak, B., Siebert, H., Brück, W., Stadelmann, C., 2017. Relationship of acute axonal damage, Wallerian degeneration, and clinical disability in multiple sclerosis. J. Neuroinflammation 14, 57.
Sorbara, C.D., Wagner, N.E., Ladwig, A., Nikić, I., Merkler, D., Kleele, T., Marinković, P., Naumann, R., Godinho, L., Bareyre, F.M., Bishop, D., Misgeld, T., Kerschensteiner, M., 2014. Pervasive axonal transport deficits in multiple sclerosis models. Neuron 84, 1183–1190.
Stankiewicz, J.M., Neema, M., Ceccarelli, A., 2014. Iron and multiple sclerosis. Neurobiol. Aging 35 (Suppl. 2), S51–S58.
Thorburne, S.K., Juurlink, B.H., 1996. Low glutathione and high iron govern the susceptibility of oligodendroglial precursors to oxidative stress. J. Neurochem. 67, 1014–1022.
Todorich, B., Pasquini, J.M., Garcia, C.I., Paez, P.M., Connor, J.R., 2009. Oligodendrocytes and myelination: the role of iron. Glia 57, 467–478.
Whitehead, M.J., McCanney, G.A., Willison, H.J., Barnett, S.C., 2019. MyelinJ: an ImageJ macro for high throughput analysis of myelinating cultures. Bioinformatics 35, 4528–4530.
Xu, X., Song, N., Wang, R., Jiang, H., Xie, J., 2016. Preferential heme oxygenase-1 activation in striatal astrocytes antagonizes dopaminergic neuron degeneration in MPTP-intoxicated mice. Mol. Neurobiol. 53, 5056–5065.
Yamada, M., Ivanova, A., Yamaguchi, Y., Lees, M.B., Ikenaka, K., 1999. Proteolipid protein gene product can be secreted and exhibit biological activity during early development. J. Neurosci. 19, 2143–2151.
Yanatori, I., Tabuchi, M., Kawai, Y., Yasui, Y., Akagi, R., Kishi, F., 2010. Heme and non-heme iron transporters in non-polarized and polarized cells. BMC Cell Biol. 11, 39.
Yu, X., Song, N., Guo, X., Jiang, H., Zhang, H., Xie, J., 2016. Differences in vulnerability of neurons and astrocytes to heme oxygenase-1 modulation: implications for mitochondrial ferritin. Sci. Rep. 6, 24200.
Zarruk, J.G., Berard, J.L., Passos dos Santos, R., Kroner, A., Lee, J., Arosio, P., David, S., 2015. Expression of iron homeostasis proteins in the spinal cord in experimental autoimmune encephalomyelitis and their implications for iron accumulation. Neurobiol. Dis. 81, 93–107.
Zhang, X., Haaf, M., Todorich, B., Grosstephan, E., Schieremberg, H., Surguladze, N., Connor, J.R., 2005. Cytokine toxicity to oligodendrocyte precursors is mediated by iron. Glia 52, 199–208.
Zhang, X., Surguladze, N., Slagle-Webb, B., Cozzi, A., Connor, J.R., 2006. Cellular iron status influences the functional relationship between microglia and oligodendrocytes. Glia 54, 795–804.
Zhang, Y., Chen, K., Sloan, S.A., Bennett, M.L., Scholze, A.R., O'Keeffe, S., Phatnani, H.P., Guarnieri, P., Caneda, C., Ruderisch, N., Deng, S., Liddelow, S.A., Zhang, C., Daneman, R., Maniatis, T., Barres, B.A., Wu, J.Q., 2014. An RNA-sequencing transcriptome and splicing database of glia, neurons, and vascular cells of the cerebral cortex. J. Neurosci. 34, 11929–11947.
Zhou, Y.F., Zhang, C., Yang, G., Qian, Z.M., Zhang, M.W., Ma, J., Zhang, F.L., Ke, Y., 2017. Hepcidin protects neuron from hemin-mediated injury by reducing Iron. Front. Physiol. 8, 332.
Zille, M., Karuppagounder, S.S., Chen, Y., Gough, P.J., Bertin, J., Finger, J., Milner, T.A., Jonas, E.A., Ratan, R.R., 2017. Neuronal death after hemorrhagic stroke in vitro and in vivo shares features of ferroptosis and necroptosis. Stroke 48, 1033–1043.
Zivadinov, R., Ramasamy, D.P., Benedict, R.R., Polak, P., Hagemeier, J., Magnano, C., Dwyer, M.G., Bergsland, N., Bertolino, N., Weinstock-Guttman, B., Kolb, C., Hojnacki, D., Utriainen, D., Haacke, E.M., Schweser, F., 2016. Cerebral microbleeds in multiple sclerosis evaluated on susceptibility-weighted images and quantitative susceptibility maps: a case-control study. Radiology 281, 884–895.
Zrzavy, T., Hametner, S., Wimmer, I., Butovsky, O., Weiner, H.L., Lassmann, H., 2017. Loss of 'homeostatic' microglia and patterns of their activation in active multiple sclerosis. Brain 140, 1900–1913.